Highly hydrophobic zeolite ZSM-8 with perfect framework structure obtained in a strongly acidic medium

Yiqing Sun, Qiaolin Lang, Guangying Fu, Haonuan Zhao, Eddy Dib, Xiaolong Liu, Xiaobo Yang, Peng Lu, Bing Yu, Valentin Valtchev

Highly hydrophobic zeolite ZSM-8 with perfect framework structure obtained in a strongly acidic medium

Yiqing Sun,[a,b] Qiaolin Lang,[b] Guangying Fu,[b] Haonuan Zhao,[c] Eddy Dib,[c] Xiaolong Liu,[a,b] Xiaobo Yang,[b*] Peng Lu,[b] Bing Yu,[a*] Valentin Valtchev [b,c*]

[a] College of Chemistry and Chemical Engineering, Qingdao University, CN-266071 Qingdao, China

[b] The ZeoMat Group, Qingdao Institute of Bioenergy and Bioprocess Technology, CAS, Laoshan District, CN-266101 Qingdao, China.

[c] Normandy University, ENSICAEN, UNICAEN, CNRS, Laboratoire Catalyse et Spectrochimie, F-14000 Caen, France.

E-mail: valentin.valtchev@ensicaen.fr, yangxb@qibebt.ac.cn, yubing198@qdu.edu.cn.

Abstract

The synthesis of zeolites in a strongly acidic medium is a new and nearly unexplored chemistry field. In addition to the previously reported silicalite-1 and the several clathrasils, this paper elaborates that one more material of unique properties could be successfully crystallized in the strongly acidic fluoride medium. A pure-silica zeolite ZSM-8 has been obtained using tetraethylammonium ion as a structure-directing agent. Rietveld refinement proves that ZSM-8 is of the **MFI** topology, i.e., it is another silicalite-1 but different in framework distortions. Moreover, the discrete and uniform crystals of the acidic-medium synthesized pure-silica ZSM-8 possess a substantially perfect framework structure and thus hydrophobic surfaces. This remarkable character renders the material an ideal adsorbent for discriminating molecules on the polarity basis, which is desired in developing green separation processes. C_3H_8, CH_4, and CO_2 are chosen as examples respecting their different polarities and tested for the adsorptive parameters.

Keywords: zeolite synthesis in acidic medium; pure-silica ZSM-8; hydrophobicity; green separation

Introduction

Zeolites are the most important adsorbents and catalysts in the oil refinery and petrochemical industry [1, 2]. Now, they are growingly investigated for processing renewable feedstocks [3-5], for remediation of air and water pollutions [6, 7], as advanced functional materials [8], as well as for medicine deliveries [9]. The applications of zeolites are based on the fundament that the uniform micropores delineated by the crystalline structure possess unique surface and diffusion properties that discriminate molecules according to their sizes and polarities, i.e., molecular sieving. The new applications often require zeolites that work under extreme temperatures and chemical environments. Briefly, zeolitic materials with reliable stabilities, finely tuned surface characteristics and diffusion properties are needed. Therefore, reviewing and improving the synthetic methods, in order to fulfill the ever-renewed property demands, remain a long-standing research task.[10]

Traditionally, zeolites are synthesized through hydrothermal crystallization in alkaline media of pH = 9~14, where Al-rich aluminosilicate zeolites with hydrophilic surfaces and a significant fraction of acid sites are obtained [11, 12]. The introduction of organic structure-directing agents (SDA), such as alkyl-ammonium ions, into the synthetic system has been successful in creating high-silica and pure-silica zeolitic structures with hydrophobic surfaces and stronger acid sites [13, 14]. In such synthetic systems, hydroxide anion plays the role of a “mineralizer” that depolymerizes the amorphous precursors and mobilize them to generate zeolite building blocks. Due to the abundant nucleation and fast growth in the presence of hydroxide ions, the crystals possess various kinds of structural defects, such as point defects at framework T sites and associated silanol nests, T-O···H-O-T clusters at broken T-O-T bridges [15], linear displacements [16], misoriented microdomains [17], intergrown of polymorphs [18], and others. These different types of defects may lead to uncontrollable surface hydrophilicity or random blockage of the micropores. Therefore, the development of zeolitic sorbents and catalysts often relies on trial-and-error experiments, rather than on theoretical deductions from the structure and composition.

Significant improvements in the crystal quality were achieved when fluoride was discovered to be able to act as a mineralizer in zeolite crystallization instead of hydroxide ions. In the “fluoride route” synthesis, the zeolite crystallization occurs

from the hydrogels containing the usual alumina and silica sources, the SDA, and the fluoride anion at pH = 5.5~8.0 [19-21]. The fluoride ion presents several advantages as a mineralizer, such as generating high-silica and pure-silica zeolites with large crystal sizes and hydrophobic surfaces. Most noticeably, the products of the fluoride route possess ordered structures that are substantially "defect-free" [22, 23].

These advantages become even more pronounced when the pH of the synthetic medium expands further to the strongly acidic region [24]. We have recently demonstrated a synthesis and morphology control method for silicalite-1, i.e., the pure-silica ZSM-5, and some other microporous silicate materials in the pH range of 2~5 [24-28]. The method is based on the fact that the silicate species' isoelectronic point in such systems bears a value of ca. pH = 2.3. Above this point, the zeolite synthesis paradigm applies that the positively charged SDA and negatively charged silicates interact and facilitate the crystallization of the target zeolites. The high solubility of low-weight hexafluoro-silicates in acidic solutions favours a slow deposition of silicate units to the growing surfaces. Thus, the product has a perfect structure without point defects [24, 25]. The crystals obtained in acidic systems have "giant" sizes of hundreds of micrometers, but can be tuned down to a few hundred nanometers through seeding with colloidal nano-crystals without ruining the high order of the framework [25].

Hydrothermal crystallization in the acidic medium generally applies to synthesizing diverse zeolites. It enables the use of those SDA and structural building blocks that are unfeasible in the traditional basic and neutral systems, thus providing opportunities for materials of new structures and new compositions [26]. The present paper elaborates the further exploration in the acidic medium using tetraethylammonium ion (TEA^+) as an SDA. TEA^+ is a versatile SDA that delivers more than 15 different zeolites in the aluminum silicate system, including zeolite beta [18], ZSM-5 [29], ZSM-8 [30], ZSM-12 [31], RHO, ZK-5, Offretite [32], and others. Now we present one more successful example for TEA^+ as an SDA in the strongly acidic medium at pH = 2.9 to 4.8 where crystals of an **MFI**-type material, i.e, a distinguished pure-silica $|TEA^+, F^-|[SiO_2]$-ZSM-8, has been obtained with a perfect framework structure and hydrophobic surface. We have tested the adsorption parameters of C_3H_8, CH_4, and CO_2. The data suggest that the acidic medium obtained ZSM-8 provides an ideal adsorbent for separating polar and apolar molecules.

Experimental

2.1 Synthesis

Chemical reagents used for the synthesis of ZSM-8 in an acidic medium were tetraethylammonium bromide (TEABr, Sigma-Alrich, 99%), fumed silica (Macklin, 98%), Ludox AS40 (Sigma-Aldrich, colloidal silica 40 wt.% aq., SiO_2/NaOH ~200), ammonium fluoride (Aladin, 98%), and hydrofluoric acid (Aladin, 40%). Table 1 lists the compositions of the initial gels, the pH values, and the hydrothermal conditions.

The syntheses in the acidic medium were carried out according to the following procedure: TEABr, NH_4F, and HF were dissolved in the calculated amount of water. Fumed silica was added to the solution and stirred at room temperature for 16 hours. The resultant hydrogels had molar compositions 1 SiO_2: 0.3 TEABr: (0.1-0.3) NH_4F: (0.2-0.4) HF: 5 H_2O, and pH values of 2.9-4.8. The gels were heated in a tumbling oven at 160^{o}C for 30 days. The solid products were decanted, thoroughly washed, and dried at 80^{o}C in air. Calcination was performed in ambient air at 550^{o}C for 12 hours.

Ref#A1 were silicalite-1 prepared in a neutral medium following the recipe 1 SiO_2: 0.3 TPABr: 0.16 NH_4F: 0.36HF: 30 H_2O (gel pH = 2.8), with Ludox AS40 as the silica source at 160°C in 10 days.

Table 1. The compositions of the initial gels, the hydrothermal conditions, and crystal morphology.

Sample	Gel composition	Gel pH	Hydrothermal condition	Morphology
A48	1 SiO_2: 0.3TEABr: 0.34NH_4F: 0.25HF: 5H_2O	4.8	160^{o}C, 30 days, tumbling	30 μm long sticks
A38	1 SiO_2: 0.3TEABr: 0.22NH_4F: 0.33HF: 5H_2O	3.8	160^{o}C, 30 days, tumbling	30 μm long sticks
A32	1 SiO_2: 0.3TEABr: 0.17NH_4F: 0.38HF: 5H_2O	3.2	160^{o}C, 30 days, tumbling	30 μm long sticks
A29	1 SiO_2: 0.3TEABr: 0.14NH_4F: 0.40HF: 5H_2O	2.9	160^{o}C, 30 days, tumbling	30 μm long sticks
Ref#A1	1 SiO_2: 0.5 TPABr: 0.16 NH_4F: 0.36 HF: 30 H_2O	2.8	160^{o}C, 10 days, static	50 μm blades

2.2 Characterization

Powder X-ray diffraction was performed on a Rigaku SmartLab diffractometer using Cu Kα radiation at 40 kV and 150 mA. An 1D detector was used to collect diffraction

data in a continuous scan mode in theta-theta geometry in the 2θ range of 5-50° for the purpose of phase identification. Zeolite samples are pressed on glass plate sample holders. High-resolution XRD data for Rietveld refinements were collected upon calcined and finely ground samples by the same diffractometer using a point detector in a step scan mode, at 0.01° steps from 5 to 120° in 2θ. GSAS-II software was applied to perform the Rietveld refinement [33]. The procedures treating the experimental and instrumental parameters were the same as the ones illustrated before [26, 34, 35].

SEM images of powder samples were taken on JEOL JSM 7900F Scanning Electron Microscope, equipped with a field emission gun operating at 5 kV. The samples were dusted on carbon sheets and inspected without coating.

FTIR spectra were recorded using Brucker Vertex 70V Spectrometer at a spectral resolution of 4 cm^{-1}. Self-sustaining pellets of the density 15 mg/cm^2 are enclosed in a gas-tight and heated cell with CaF_2 windows. Spectra were recorded after dehydrations in 30 ml/min flowing Ar at 25, 125, 200, 350, and 500^oC for 30 min, respectively.

TG/DTA analysis was performed using Rigaku TG-DTA8122 microbalance upon ca. 10 mg zeolite powder against α-Al_2O_3, in 50 ml/min reconstituted (80% N_2 + 20% O_2) airflow at a heating rate of 10^oC/min.

^{29}Si MAS NMR experiments were performed on Bruker AVANCE III 600 spectrometer at a resonance frequency of 119.2 MHz. The spectra with high-power proton decoupling were recorded on a 4 mm probe with a spinning rate of 10 kHz, a $\pi/4$ pulse length of 2.6 μs, and a recycle delay of 60 s. The chemical shifts of ^{29}Si are referenced to TMS. The fitting of the NMR spectra is done using Dmfit software [36].

Ar adsorption/desorption isotherm was measured at 87 K using a Quantachrome Autosorb-iQ system. C_3H_8, CH_4, and CO_2 adsorption isotherms at 303-373 K were measured using the same equipment.

Results and Discussions

3.1 Crystallinity and morphology of ZSM-8

The powder XRD patterns (Figure 1a) of the crystals obtained in the pH range of 2.8-

4.8 with TEA^+ as the SDA show that the 4 samples belong to the same phase that was named ZSM-8. ZSM-8 was prepared in high-silica and pure-silica versions in the presence of TEA^+ [29, 37, 38]. The patterns are also similar to the ones of **MFI**-type silicalite-1 crystallized using tetra-propylammonium SDA [14]. There are no significant differences between ZSM-8 and ZSM-5 in XRD, in particular on the relative intensities of the peaks. Figure 1b compares two high-resolution XRD patterns of ZSM-8 (Sample #A29) and silicalite-1 (Ref#A1), both have been synthesized in the acidic medium at pH near 3 and ground carefully for the X-ray diffraction data collection. SEM images in Figure 2 confirm that the ZSM-8 powders consist of discrete and uniform crystals of acicular-prismatic shapes around 30-50 μm

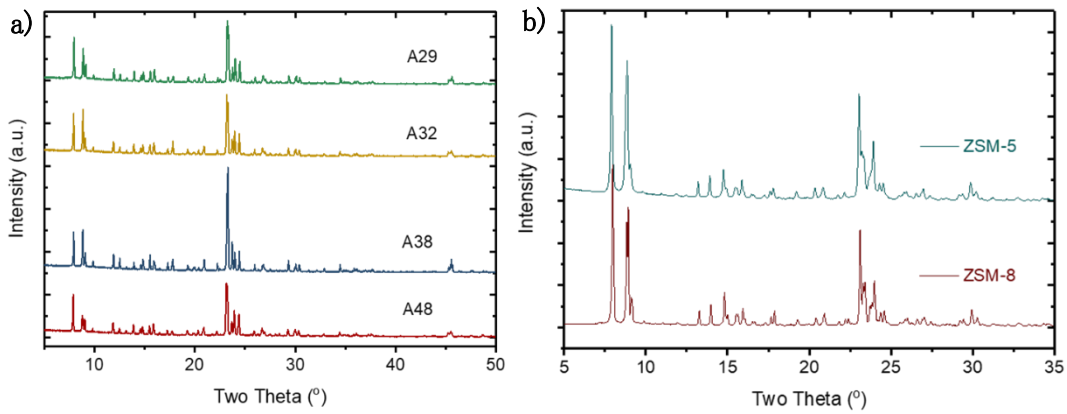

in length. Intergrowths of the crystals are occasionally seen. With decreasing gel pH, the crystals become slightly longer and thicker.

Figure 1: The XRD patterns (a) of as-synthesized |TEA^+|-ZSM-8 samples, A48-A29, as in Table 1; and (b) of ZSM-8 (A29) and silicalite-1 (Ref#A1) fine-ground powders, both synthesized at pH near 3.

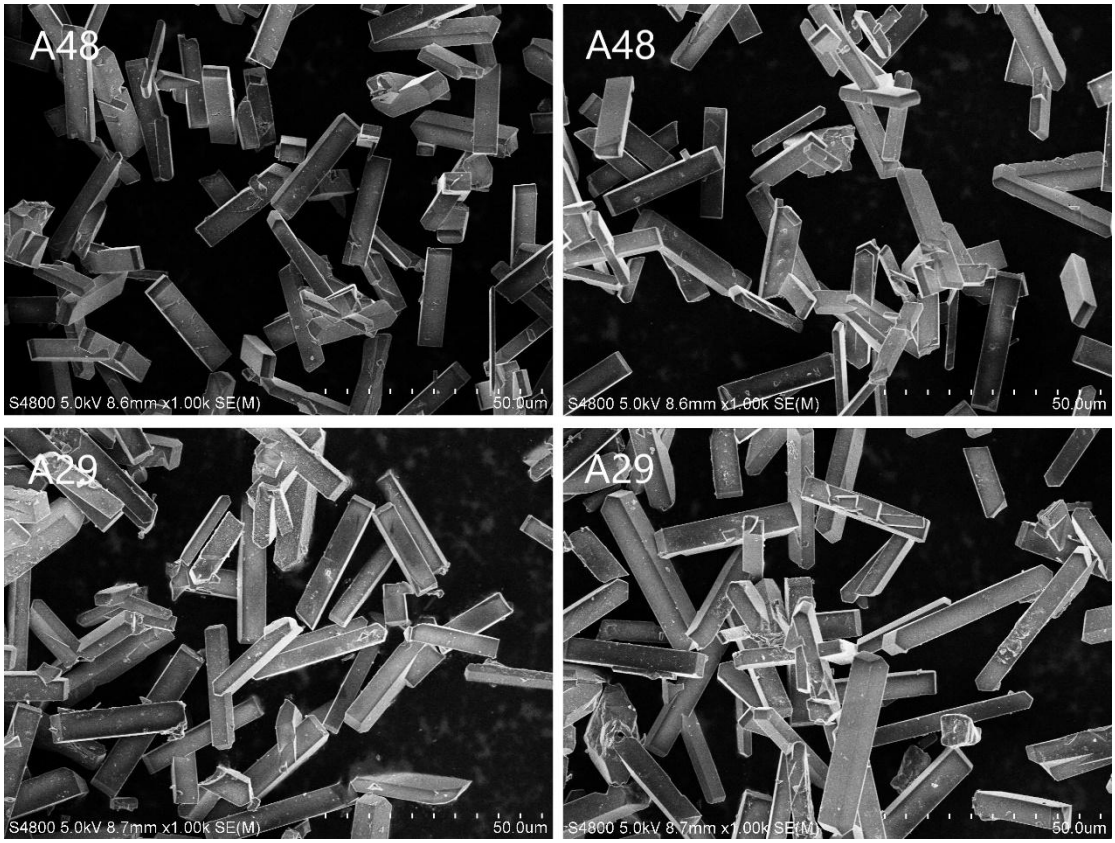

Figure 2: SEM images of |TEA^+|-ZSM-8 samples, A48 and A29 as in Table 1.

The earlier literature distinguished ZSM-8 from ZSM-5 based on several arguments, such as shifts and splitting of powder diffraction peaks [37], different IR bands in the framework fingerprint region [30], different temperature profiles of SDA combustion [39], different adsorption capacities of small organic molecules [30, 37, 40], etc. However, none of them was sufficient to define that ZSM-8 has a distinctive framework topology. Figure 3 shows TG-DTA curves of the as-synthesized and calcined samples A48 and A29. The as-synthesized samples show similar weight-loss processes in the air, with the same heat effects. Indeed, they show an unusual process of SDA combustion. In addition to a major weight loss of 8.5 % at ca. 400^{o}C with a significant exothermic peak, further exothermic weight losses of 2.5 % extends to around 700^{o}C. The combustion process of TEA^+ cations from ZSM-8 differs significantly from the combustion of TPA^+ from silicalite-1, which is known to follow only one simple step and is complete, usually below 500^{o}C [25]. Hence, TEA^+ exhibits stronger interactions with the framework of ZSM-8.

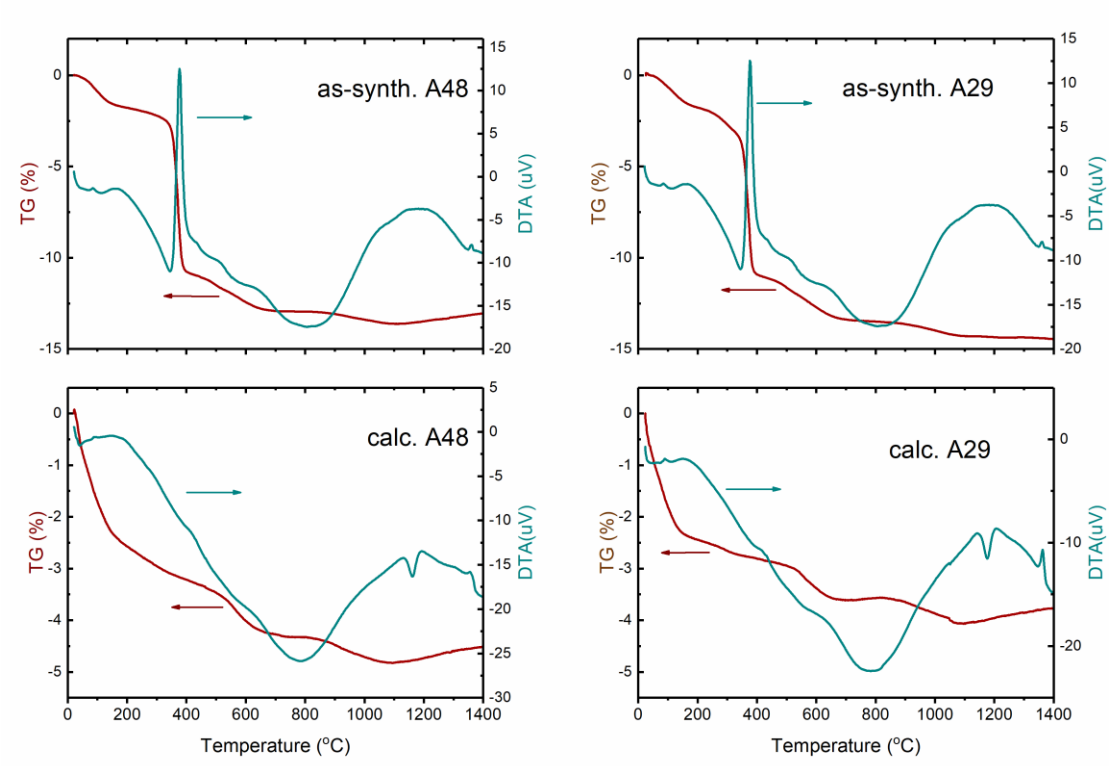

Figure 3：TG/DTA of the as-synthesized and calcined |TEA^+|-ZSM-8 samples.

Despite the differences in XRD and TG/DTA, Weidenthaler et al. pointed out that the framework topology of ZSM-8 is identical to that of ZSM-5 based on Rietveld refinement. It means that ZSM-8 is another **MFI**-type material [30]. Many other authors, e.g., Zhao et al., synthesized high-silica zeolites in the presence of TEA^+ and TPA^+, respectively, and did not differentiate their structures [29]. It was also suggested that ZSM-8 belongs to the pentasil family, which consists of intergrown **MFI** and **MEL** by stacking the same layered unit in different sequences [39, 41, 42]. However, our attempt to fit the high-resolution XRD pattern of calcined A29 sample using DIFFaX [43] failed at any mixing ratios of **MFI** and **MEL** topologies, indicating that the material is not an intergrown of the two distinct structures. On the other hand, our Rietveld refinements also prove that the pure-silica ZSM-8 from the acidic-medium synthesis possess **MFI** topology, albeit the different peak shapes and intensities. High-resolution XRD patterns of two selected samples have been chosen to perform the Rietveld refinements. The samples are the pure-silica ZSM-8 synthesized at pH = 2.9 (calcined A29), and a reference silicalite-1 sample Ref#A1 synthesized at pH = 2.8 using TPA^+ as the SDA. The reference sample is a typical silicalite-1 with a well-known blade-like morphology of edge lengths at 50-60

microns [25]. The Rietveld conditions and results for both samples are compared in Table 2. The fitted XRD patterns, the atomic coordinates, and more structural details are presented in the Supporting Information and as Crystallographic Information Files (.cif) deposited at CCDC, #2262304 and 2262305, respectively.

Table 1. Experimental conditions (Sample A29 and Ref#A1) and crystallographic parameters pertaining to the Rietveld refinement.

	A29 (ZSM-8)	Ref#A1 (Silicalite-1)
Wavelength (Å)	1.540510/1.544330 (Cu Kα)	1.540510/1.544330 (Cu Kα)
Temperature (K)	298	298
2θ Range (^{o})	5-120 (6-119 used)	5-120 (6-119 used)
Step size (^{o})	0.01	0.01
No. of observations	11301	11301
No. of variables	258	257
Space group	$P2_1/n$ (#14)	$P2_1/n$ (#14)
Unit cell parameters		
a (Å)	19.8948(4)	19.9074(5)
b (Å)	20.1191(3)	20.1320(4)
c (Å)	13.3856(3)	13.3943(4)
β (^{o})	90.573(2)	90.599(3)
Cell volume (Å^3)	5357.5(2)	5367.8(3)
Residuals		
R_{wp}	0.1166	0.08465
R_p	0.0337	0.0356
R_F^2	0.1422	0.1271
Reduced χ^2	1.79	2.76

The data in Table 2 show that the refinements converge at a similar unit cell geometry for both materials in the same space group $P2_1/n$, #14, with the same **MFI** topology. ZSM-8 has a slightly smaller unit cell volume, with contractions in all three edge lengths but almost the same angle in β. The pure-silica ZSM-8 crystallized in the strongly acidic medium is another silicalite-1, with a slightly shrinking and more distorted framework structure. This is in accordance with the observation of Weidenthaler et al. for the aluminosilicate version of ZSM-8 crystallized in the traditional basic medium [30]. The (almost) same unit cell geometry, along with the same space group, imposes no peak splitting of ZSM-8 if compared to Silicalite-1. What looks like "splitting" is likely only the effect of shorter FWHM, which emulates a splitting of almost overlapped (but independent) Bragg peaks. This is reasonable for very long unit-cell edges, and somehow reflects even a very good crystallinity of the

ZSM-8 sample.

3.2 Framework structure and hydrophobicity

Figure 4 shows the ^{29}Si MAS NMR of sample A29. The spectrum displays high resolutions for Q^4 (Si-$(OSi)_4$) signals in the range of -105~-120 ppm. Peak fitting can discriminate 11 groups of Q^4 resonances. For **MFI** topology, there are 12 unique crystallographic T sites in the orthorhombic unit cell (*Pnma* #62) or 24 T sites in the monoclinic unit cell ($P2_1/n$ #14). Such a high resolution in ^{29}Si MAS NMR has been achieved only once for all zeolites ever, which was the |TPA^+|-silicalite-1 materials synthesized at pH around 3 [25]. Therefore, the highly ordered structure is the specific feature for zeolites crystallized in the strongly acidic medium. In addition, there is one broadband at -127 ppm, the so-called Q^5 $(SiO)_4$-Si···F, corresponding to the Si atoms of the [$4^1 5^2 6^2$] cage that interact with F^- ion entrapped in the cage.[44]

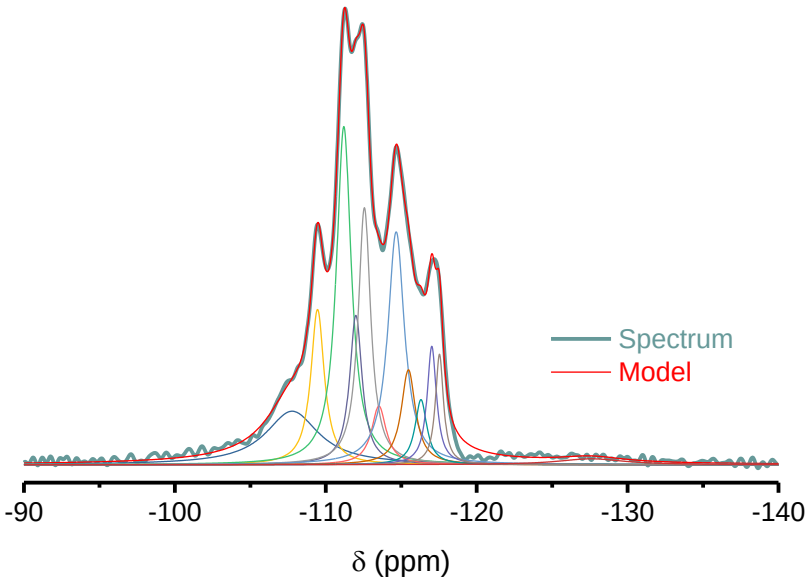

Figure 4: ^{29}Si MAS NMR of |TEA^+|-ZSM-8 sample synthesized in the strongly acidic medium (Sample A29).

Figure 5 are the FTIR spectra of calcined ZSM-8 samples (A48 and A29) in the -OH vibration region, recorded after dehydration at increasing temperatures in Ar flow. At the hydrated state, sample A48 shows a broad absorption band at 3670 cm^{-1}, corresponding to the stretching vibration of surface silanol groups that are H-bonded

with adsorbed H_2O; another weaker band at 3440 cm^{-1}, arose from the adsorbed H_2O molecules inside the zeolite channels. Upon dehydration, the 3440 cm^{-1} band disappears; the 3670 cm^{-1} blue-shifts and loses its intensity. It settles as a peak at 3740 cm^{-1} when the samples become fully dehydrated at 500°C. Sample A29 shows the same peaks at even lower absorbance values. The remaining peaks after dehydration at 500°C are almost at the same level as the spectroscopic noises. The material is highly hydrophobic, and is saturated with only a small amount of water in the ambient air at ambient temperature.

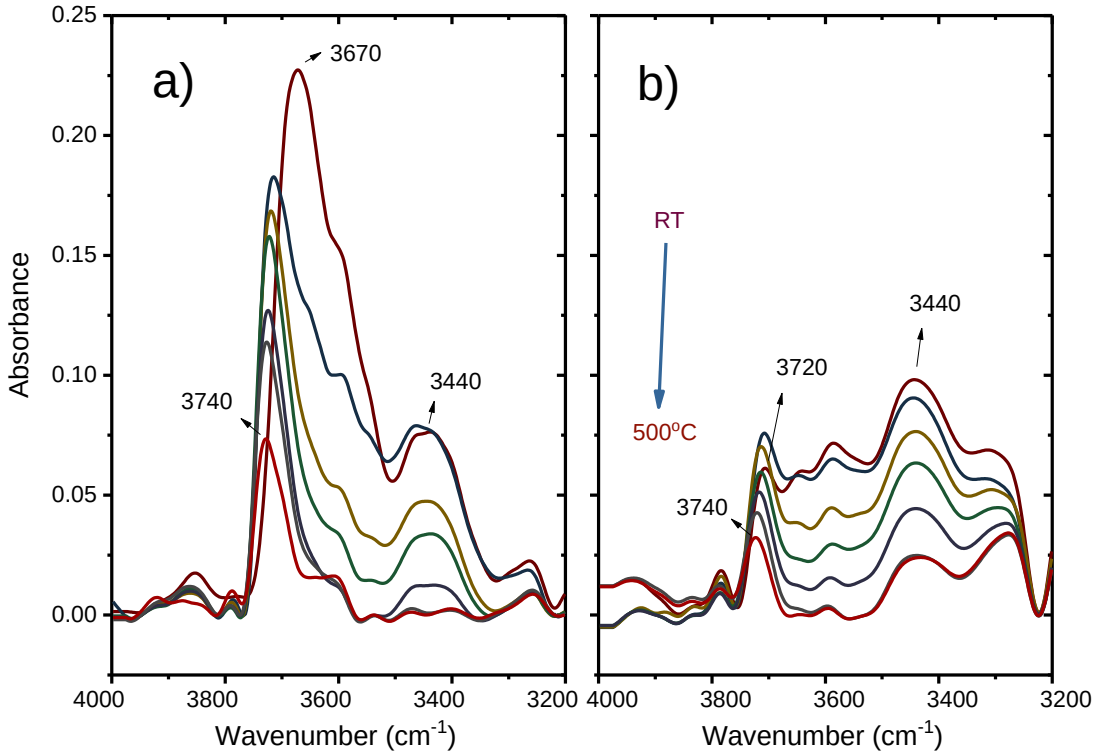

Figure 5: FTIR spectra of calcined pure-silica ZSM-8 samples A48 (a) and A29 (b) that dehydrated at up to 500°C in Ar flow.

Referring to the TG/DTA curves of the calcined and rehydrated samples in Figure 3, the saturated H_2O adsorption amount, regarding the weight losses up to 500°C is ca. 3.5 wt% for A48, and ca. 3.0 wt% for A29. Furthermore, there is less than 1 wt% weight loss due to the silanol condensation at around 600°C for both samples. TG/DTA reveals the hydrophobic nature of the material again. DTA further reveals that ZSM-8's framework collapses at 1180°C. At 1370°C alpha-quartz crystallizes from the mass.

3.3 Adsorption of Ar, C_3H_8, CH_4, and CO_2

Figure 6 presents Ar adsorption isotherms at 87 K of ZSM-8 samples calcined at 550°C. According to the IUPAC classification, they are ascribed to the type I with a steep increment in the adsorbed amount at $P/P_0 < 1\times10^{-2}$, followed by a plateau until saturation. This is typical for microporous materials. t-plot (de Boer) micropore (< 2 nm) volumes have been calculated at 0.14-0.17 cm^3/g from the isotherm data. Ar at 87 K has been chosen for the adsorption measurement, instead of N_2 at 79 K, because according to IUPAC recommendation, the fast filling of 0.5-1.0 nm pores with Ar occurs at higher P/P_0 (10^{-5}~10^{-3}, vs. 10^{-7}~10^{-5}), which fact eases more accurate experiments; and the interaction of N_2 quadrupole with the oxidic functional groups of zeolite framework is eliminated [45, 46].

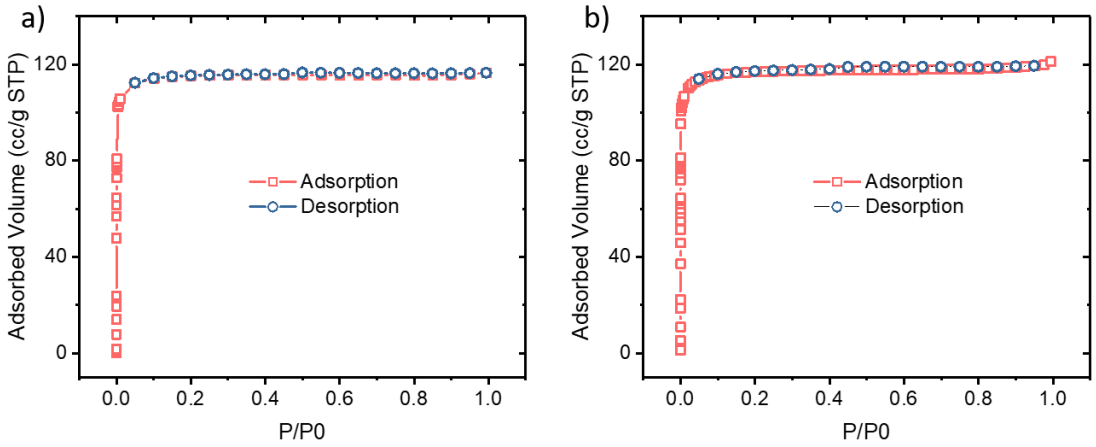

Figure 6: Ar adsorption isotherms at 87 K for ZSM-8: (a) Sample A48, (b) Sample A29.

Figure 7 shows C_3H_8, CH_4, and CO_2 adsorption isotherms at 303-373 K over sample A29. The isotherm of C_3H_8 is of Type I, and shows steep increments at low pressures. CH_4 and CO_2 isotherms show monotonic increments with the pressure, but grow slowly. The CH_4 adsorbed amount is obviously lower. Table 3 reports the Langmuir fitting results of these isotherms [47, 48], and the isosteric adsorption heat calculated for the coverage of $\theta = 0.4$ according to Clausius-Clapeyron Equation.

The micropore of ZSM-8 has a higher affinity to C_3H_8 and CH_4 than CO_2, respecting the adsorption heats. The isosteric adsorption heats for the paraffin molecules are 36.8 and 38.7 kJ/mol, while the one for CO_2 is only 19.0 kJ/mol. The difference is

significant for designing processes for their separations. The 1st order Langmuir equation assumes a homogeneous adsorption surface with only one type of equal adsorption sites. Therefore, the calculated ln(P) vs. 1/T lines for various coverages (θ) are strictly parallel, with a single ΔH_{st} value as the slops in the Clausius-Clapeyron equation, $lnP = -\Delta H_{st}/RT + c$ (Figure S3). The experimental data points show some deviations from the 1st order Langmuir fittings. Figure S4 shows, e.g., the adsorption isotherms for C_3H_8 represented as ln(P) vs coverages (θ), calculated based on Langmuir infinitive Q. Picking data points from these isotherms to calculate the dependency of ΔH_{st} on θ, one can see the discrepancies due to heterogeneities of the adsorption sites. In particular, ΔH_{st} values at lower coverages have higher but sometimes tubulating values, because the first adsorptions occur at stronger sites. The ΔH_{st} values stabilize and decrease slightly at moderate to full coverages. The same procedure of data interpretation has been applied to CH_4 and CO_2, too. The curves are presented as well in Figure S4. They show in principle the same trends of deviations. However, the data points cover only the lower ends of θ for these two adsorbates.

In the experimental range the adsorption isotherms of C_3H_8 appear very differently from CH_4. ZSM-8 shows good affinity to C_3H_8 at low pressures. All isotherms in the tested temperature range show obvious inflexions. The Henry's constants for C_3H_8 in the low-pressure ranges bares apparently much bigger values than for CH_4. Still, the first-order Langmuir equations provide satisfactory fittings, and reveals similar ΔH_{st} for C_3H_8 and CH_4. When looking at the vdW contribution to the enthalpy of adsorption of alkanes, Lewellyn et al. showed that each CH_2 contributes to around 9 kJ/mol to the overall adsorption enthalpy [49, 50]. The different behaviors of zeolites in the adsorption of light alkanes may be attributed to the small-sized, yet periodically structured micropores, in ZSM-8 only ca. 0.6 nm in diameter, which offer discrete adsorption sites in specific geometrical locations for the particular adsorbate to access.

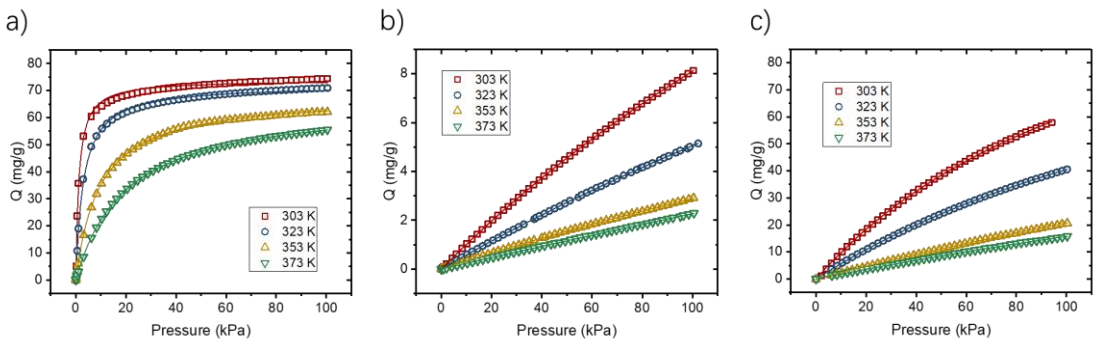

Figure 7: C_3H_8 (a), CH_4 (b) and CO_2 (c) adsorption isotherms of the ZSM-8 Sample A29.

Table 3. The Langmuir parameters of C_3H_8 and CO_2 adsorption isotherms for ZSM-8 (Sample A29) and the isosteric adsorption heat at θ = 0.4 calculated by Clausius-Clapeyron Equation.

	C_3H_8			CH_4			CO_2		
	$Q = Q_{inf} k P/(1+k P)$		$lnP = -\Delta H_{st}/RT + c$	$Q = Q_{inf} k P/(1+k P)$		$lnP = -\Delta H_{st}/RT + c$	$Q = Q_{inf} k P/(1+k P)$		$lnP = -\Delta H_{st}/RT + c$
T (K)	Q_{inf} (mg/g)	k (kPa^{-1})	ΔH_{st} (kJ/mol)	Q_{inf} (mg/g)	k (kPa^{-1})	ΔH_{st} (kJ/mol)	Q_{inf} (mg/g)	k (kPa^{-1})	ΔH_{st} (kJ/mol)
303	73.92	0.796	36.8	37.50	0.00276	38.7	140.95	0.00748	19.0
323	72.18	0.330		34.51	0.00172		126.85	0.00469	
353	68.24	0.106		19.99	0.00169		109.66	0.00244	
373	66.42	0.050		16.49	0.00147		102.50	0.00182	

Conclusions

The crystallization of high silica and pure silica zeolites in an acidic fluoride medium has rarely been investigated. Still, it is a vast chemistry field to be explored for new structures and chemical compositions that offer new properties for novel applications. We have been initiating in-depth studies of acidic medium synthesis of zeolites recently. As a first success, we have been able to demonstrate that **MFI** of Si/Al > ca. 100 crystallizes out of various silica sources using tetra-propylammonium as SDA in the acidic medium of pH closing 2. Lately, we exhibited that the acidic-medium synthesis is not a one-time case for **MFI**, but is a proven method generally applicable for high silica polymorphs.

The present paper illustrates the crystallization of pure-silica ZSM-8 in an acidic medium using tetraethylammonium as SDA. ZSM-8 has the **MFI** framework

topology but differs from silicalite-1 in a moderate structure distortion, via tetrahedra tilting. The acidic-medium synthesized ZSM-8 has a perfect structure with high local orders, therefore, highly hydrophobic surfaces. C_3H_8, CH_4 and CO_2 have been used as representatives of small gas molecules of different polarities and demonstrated the ability of ZSM-8 in gas adsorption.

Author Contributions

Y. Sun, Q. Lang, G. Fu, **H. Zhao, E. Dib, X. Liu**: Investigation. **X. Yang**: Conceptualization, Supervision, Methodology, Investigation, Writing – original draft. **P. Lu, B. Yu:** Supervision. **V. Valtchev**: Conceptualization, Supervision, Writing – review & editing, Funding acquisition.

Acknowledgments

The ZeoMat Group acknowledges the starting grant provided by QIBEBT, the support provided by the Shandong Energy Institute, and the Nature Science Foundation of Shandong Province. VV, XY, and PL acknowledge the collaboration under the Sino-French International Research Network (IRN) "Zeolites".

Funding

Shandong Energy Institute (SEI S202107), Nature Science Foundation of Shandong Province (ZR2022MB053 and ZR2022QB216).

References

[1] C. Martínez, A. Corma, Inorganic molecular sieves: Preparation, modification and industrial application in catalytic processes, Coordination Chemistry Reviews, 255 (2011) 1558-1580.

[2] R.M. Barrer, Zeolites and their synthesis, Zeolites, 1 (1981) 130-140.

[3] B. Yilmaz, U. Müller, Zeolites Catalyzing Raw Material Change for a Sustainable Chemical Industry, in: F.-S. Xiao, X. Meng (Eds.) Zeolites in Sustainable Chemistry: Synthesis, Characterization and Catalytic Applications, Springer Berlin Heidelberg, Berlin, Heidelberg, 2016, pp. 473-480.

[4] Y. Li, L. Li, J. Yu, Applications of Zeolites in Sustainable Chemistry, Chem, 3 (2017) 928-949.

[5] E. Taarning, C.M. Osmundsen, X. Yang, B. Voss, S.I. Andersen, C.H.

Christensen, Zeolite-catalyzed biomass conversion to fuels and chemicals, Energy & Environmental Science, 4 (2011) 793-804.
[6] Y. Li, J. Yu, Emerging applications of zeolites in catalysis, separation and host–guest assembly, Nature Reviews Materials, (2021).
[7] B. Yilmaz, U. Müller, Catalytic Applications of Zeolites in Chemical Industry, Topics in Catalysis, 52 (2009) 888-895.
[8] G.A. Ozin, A. Kuperman, A. Stein, Advanced Zeolite, Materials Science, Angewandte Chemie International Edition in English, 28 (1989) 359-376.
[9] M. Zaarour, B. Dong, I. Naydenova, R. Retoux, S. Mintova, Progress in zeolite synthesis promotes advanced applications, Microporous and Mesoporous Materials, 189 (2014) 11-21.
[10] E.B. Clatworthy, S.V. Konnov, F. Dubray, N. Nesterenko, J.P. Gilson, S. Mintova, Emphasis on the Properties of Metal‐Containing Zeolites Operating Outside the Comfort Zone of Current Heterogeneous Catalytic Reactions, Angewandte Chemie International Edition, (2020).
[11] D.W. Breck, Zeolite Molecular Sieves: Structure, Chemistry, and Use, John Wiley and Sons, New York, London, Sydney, and Toronto, 1974.
[12] C.S. Cundy, P.A. Cox, The Hydrothermal Synthesis of Zeolites: History and Development from the Earliest Days to the Present Time, Chemical Reviews, 103 (2003) 663-702.
[13] G.T. Kokotailo, S.L. Lawton, D.H. Olson, W.M. Meier, Structure of synthetic zeolite ZSM-5, Nature, 272 (1978) 437-438.
[14] E.M. Flanigen, J.M. Bennett, R.W. Grose, J.P. Cohen, R.L. Patton, R.M. Kirchner, J.V. Smith, Silicalite, a new hydrophobic crystalline silica molecular sieve, Nature, 271 (1978) 512-516.
[15] I.C. Medeiros-Costa, E. Dib, N. Nesterenko, J.-P. Dath, J.-P. Gilson, S. Mintova, Silanol defect engineering and healing in zeolites: opportunities to fine-tune their properties and performances, Chemical Society Reviews, 50 (2021) 11156-11179.
[16] B.J. Campbell, A.K. Cheetham, Linear Framework Defects in Zeolite Mordenite, The Journal of Physical Chemistry B, 106 (2002) 57-62.
[17] K.N. Bozhilov, T.T. Le, Z. Qin, T. Terlier, A. Palčić, J.D. Rimer, V. Valtchev, Time-resolved dissolution elucidates the mechanism of zeolite MFI crystallization, Science Advances, 7 (2021) eabg0454.
[18] J.M. Newsam, M.M.J. Treacy, W.T. Koetsier, C.B.D. Gruyter, J.M. Thomas, Structural characterization of zeolite beta, Proceedings of the Royal Society of London. A. Mathematical and Physical Sciences, 420 (1988) 375-405.

[19] J.-L. Guth, P. Caullet, Synthèse des zéolites. Perspectives d'avenir, Journal de chimie physique, 83 (1986) 155-175.
[20] J. Guth, L. Delmonte, M. Soulard, B. Brunard, J. Joly, D. Espinat, Synthesis of Al, Si · MFI-type zeolites in the presence of F− anions: Structural and physicochemical characteristics, Zeolites, 12 (1992) 929-935.
[21] M. A. Camblor, A. Corma, S. Valencia, Synthesis in fluoride media and characterisation of aluminosilicate zeolite beta, Journal of Materials Chemistry, 8 (1998) 2137-2145.
[22] P. Caullet, J.-L. Paillaud, A. Simon-Masseron, M. Soulard, J. Patarin, The fluoride route: a strategy to crystalline porous materials, Comptes Rendus Chimie, 8 (2005) 245-266.
[23] M.A. Camblor, L.A. Villaescusa, M.J. Díaz-Cabañas, Synthesis of all-silica and high-silica molecular sieves in fluoride media, Topics in Catalysis, 9 (1999) 59-76.
[24] D. Shi, K.-G. Haw, C. Kouvatas, L. Tang, Y. Zhang, Q. Fang, S. Qiu, V. Valtchev, Expanding the Synthesis Field of High-Silica Zeolites, Angewandte Chemie-International Edition, 59 (2020) 19576-19581.
[25] X. Yang, E. Dib, Q. Lang, H. Guo, G. Fu, J. Wang, Q. Yi, H. Zhao, V. Valtchev, Silicalite-1 formation in acidic medium: Synthesis conditions and physicochemical properties, Microporous and Mesoporous Materials, 329 (2022) 111537.
[26] G. Fu, E. Dib, Q. Lang, H. Zhao, S. Wang, R. Ding, X. Yang, V. Valtchev, Acidic medium synthesis of zeolites – an avenue to control the structure-directing power of organic templates, Dalton Transactions, 51 (2022) 11499-11506.
[27] H. Zhao, Q. Lang, G. Fu, R. Ding, S. Wang, X. Yang, V. Valtchev, Hydrothermal crystallization of clathrasils in acidic medium: Energetic aspects, Microporous and Mesoporous Materials, 333 (2022) 111728.
[28] Q. Lang, G. Fu, H. Zhao, J. Wang, X. Yang, V. Valtchev, Biomineralization at the Molecular Level: Amino Acid-Assisted Crystallization of Zeotype AlPO4·1.5H2O–H3, Crystal Growth & Design, 21 (2021) 7298-7305.
[29] D. Zhao, S. Qiu, W. Pang, Synthesis and characterization of ZSM-5 containing tripropylammonium and tetraethylammonium cations, Zeolites, 13 (1993) 478-480.
[30] C. Weidenthaler, R.X. Fischer, R.D. Shannon, The essential identity of the framework structures of ZSM-8 and ZSM-5, in: J. Weitkamp, H.G. Karge, H. Pfeifer, W. Hölderich (Eds.) Studies in Surface Science and Catalysis, Elsevier1994, pp. 551-558.
[31] C.A. Fyfe, H. Gies, G.T. Kokotailo, B. Marler, D.E. Cox, Crystal structure of silica-ZSM-12 by the combined use of hgh-resolution solid-state MAS NMR

spectroscopy and synchrotron x-ray powder diffraction, The Journal of Physical Chemistry, 94 (1990) 3718-3721.
[32] H. Lee, J. Shin, S.B. Hong, Tetraethylammonium-Mediated Zeolite Synthesis via a Multiple Inorganic Cation Approach, ACS Materials Letters, 3 (2021) 308-312.
[33] B.H. Toby, R.B. Von Dreele, GSAS-II: the genesis of a modern open-source all purpose crystallography software package, Journal of Applied Crystallography, 46 (2013) 544-549.
[34] X. Yang, B.H. Toby, M.A. Camblor, Y. Lee, D.H. Olson, Propene adsorption sites in zeolite ITQ-12: a combined synchrotron X-ray and neutron diffraction study, J Phys Chem B, 109 (2005) 7894-7899.
[35] X. Yang, M.A. Camblor, Y. Lee, H. Liu, D.H. Olson, Synthesis and crystal structure of As-synthesized and calcined pure silica zeolite ITQ-12, J Am Chem Soc, 126 (2004) 10403-10409.
[36] D. Massiot, F. Fayon, M. Capron, I. King, S. Le Calvé, B. Alonso, J.-O. Durand, B. Bujoli, Z. Gan, G. Hoatson, Modelling one- and two-dimensional solid-state NMR spectra, Magnetic Resonance in Chemistry, 40 (2002) 70-76.
[37] C.J. Plank, E.J. Rosinski, M.K. Rubin, Crystalline zeolite and method of preparing the same, in: GB (Ed.), MOBIL OIL CORPORATION, GB, 1973.
[38] M.S. Joshi, K. Mohan Prabhu, Synthesis and characterization of ZSM-8-type zeolite crystals, Crystal Research and Technology, 23 (1988) 561-566.
[39] Z. Gabelica, E. G. Derouane, N. Blom, Synthesis and characterization of pentasil type zeolites: II. Structure-directing effect of the organic base or cation, Applied Catalysis, 5 (1983) 109-117.
[40] V.R. Choudhary, A.S. Mamman, Diffusion of cumene in H-ZSM-8 and modified H-ZSM-8 Zeolites, AIChE Journal, 36 (1990) 1577-1580.
[41] Z. Gabelica, E.G. Derouane, N. Blom, Factors Affecting the Synthesis of Pentasil Zeolites, Catalytic Materials: Relationship Between Structure and Reactivity, American Chemical Society1984, pp. 219-251.
[42] E.G. Derouane, Z. Gabelica, A novel effect of shape selectivity: Molecular traffic control in zeolite ZSM-5, Journal of Catalysis, 65 (1980) 486-489.
[43] M.M.J. Treacy, J.M. Newsam, M.W. Deem, A general recursion method for calculating diffracted intensities from crystals containing planar faults, Proceedings of the royal society A, Mathematical, physical and engineering sciences, 433 (1991) 499-520.
[44] C.A. Fyfe, D.H. Brouwer, A.R. Lewis, J.-M. Chézeau, Location of the Fluoride Ion in Tetrapropylammonium Fluoride Silicalite-1 Determined by 1H/19F/29Si Triple

Resonance CP, REDOR, and TEDOR NMR Experiments, Journal of the American Chemical Society, 123 (2001) 6882-6891.
[45] M. Thommes, K. Kaneko, A.V. Neimark, J.P. Olivier, F. Rodriguez-Reinoso, J. Rouquerol, K.S.W. Sing, Physisorption of gases, with special reference to the evaluation of surface area and pore size distribution (IUPAC Technical Report), Pure and Applied Chemistry, 87 (2015) 1051.
[46] J. Villarroel-Rocha, D. Barrera, J.J. Arroyo-Gómez, K. Sapag, Critical Overview of Textural Characterization of Zeolites by Gas Adsorption, in: S. Valencia, F. Rey (Eds.) New Developments in Adsorption/Separation of Small Molecules by Zeolites, Springer International Publishing, Cham, 2020, pp. 31-55.
[47] J.A. Thompson, S.I. Zones, Binary- and Pure-Component Adsorption of CO2, H2O, and C6H14 on SSZ-13, Industrial & Engineering Chemistry Research, 59 (2020) 18151-18159.
[48] D.H. Olson, X.B. Yang, M.A. Camblor, ITQ-12: A zeolite having temperature dependent adsorption selectivity and potential for propene separation, Journal of Physical Chemistry B, 108 (2004) 11044-11048.
[49] P.L. Llewellyn, P. Horcajada, G. Maurin, T. Devic, N. Rosenbach, S. Bourrelly, C. Serre, D. Vincent, S. Loera-Serna, Y. Filinchuk, G. Férey, Complex Adsorption of Short Linear Alkanes in the Flexible Metal-Organic-Framework MIL-53(Fe), Journal of the American Chemical Society, 131 (2009) 13002-13008.
[50] T.K. Trung, P. Trens, N. Tanchoux, S. Bourrelly, P.L. Llewellyn, S. Loera-Serna, C. Serre, T. Loiseau, F. Fajula, G. Férey, Hydrocarbon Adsorption in the Flexible Metal Organic Frameworks MIL-53(Al, Cr), Journal of the American Chemical Society, 130 (2008) 16926-16932.